Coordinated Robust PID-based Damping Control of Permanent Magnet Synchronous Generators for Low-frequency Oscillations Considering Power System Operational Uncertainties

Rehan Sadiq, Zhen Wang, *Member*, *IEEE*, Chi Yung Chung, *Fellow*, *IEEE*, Deqiang Gan, *Senior Member*, *IEEE*, and Cunzhi Tong

***Abstract*—In recent years, with the growth of wind energy resources, the capability of wind farms to damp low-frequency oscillations (LFOs) has provided a notable advantage for the stability enhancement of the modern power grid. Meanwhile, owing to variations in the power system operating point (OP), the damping characteristics of LFOs may be affected adversely. In this respect, this paper presents a coordinated robust proportional-integral-derivative (PID) based damping control approach for permanent magnet synchronous generators (PMSGs) to effectively stabilize LFOs, while considering power system operational uncertainties in the form of a polytopic model constructed by linearizing the power system under a given set of OPs. The proposed approach works by modulating the DC-link voltage control loop of the grid-side converter (GSC) via a supplementary PID controller, which is synthesized by transforming the design problem into *H*-infinity static output feedback (SOF) control methodology. The solution of *H*-infinity SOF control problem involves satisfying linear matrix inequality (LMI) constraints based on the parameter-dependent Lyapunov function to ensure asymptotic stability such that the minimal *H*-infinity performance objective is simultaneously accomplished for the entire polytope. The coordinated damping controllers for the multiple wind farms are then designed sequentially by using the proposed approach. Eigenvalue analysis confirms the improved damping characteristics of the closed-loop system for several representative OPs. Afterward, the simulation results, including the performance comparison with existing approaches, validate the higher robustness of the proposed approach for a wide range of operating scenarios.**

***Index Terms*—Permanent magnet synchronous generator (PMSG), low-frequency oscillation (LFO), proportional-integral-derivative (PID), robust control, *H*-infinity static output feedback control, linear matrix inequality (LMI).**

I. Introduction

THE low-frequency oscillations (LFOs), excited between the conventional synchronous generators (SGs), are regarded as the inherent and widely occurring oscillation types in large-scale interconnected power networks [1]. Owing to the global trend toward producing renewable and sustainable energy, wind power generation has recently emerged as a promising resource with extensive growth potential [2]. The high penetration with intermittent wind power output, on the other hand, could diminish the damping margin and further amplify LFOs, ultimately deteriorating the small-signal stability of the modern power network [3]. Therefore, noticeable attention has been devoted in the past decade to LFO damping in wind-integrated power systems [4], [5].

Among different wind turbine (WT) systems, the direct-drive permanent magnet synchronous generator (PMSG) is nowadays becoming one of the most popular and extensively utilized wind energy conversion systems [6]. Considering the wind market in China, the commissioning of the PMSG-type wind turbine generators (WTGs) is sharply growing, in particular for the off-shore wind power deployment [7]. The reason behind is their attractive features such as a gearless mechanism with less maintenance requirements and overall cost, high efficiency, and smooth operation, compared with other-type WTGs [7], [8]. This encourages the authors to employ PMSG in the proposed work as the primary control entity for the damping control action. Nevertheless, the studies involved here can be easily extended and applicable to other-type WTGs.

In this respect, exploiting the ancillary service of the PMSG via modulating its full-scale converter presents a great capability to damp LFOs [9]. For this purpose, researchers have realized various possibilities regarding the modulation of the WT converter. Active power modulation with an additional damping controller is one of the popular ways to achieve the damping objective [10]-[12]. However, it may excite the torsional oscillation of the drive train, caus-

Manuscript received: May 24, 2023; revised: July 12, 2023; accepted: July 30, 2023. Date of CrossCheck: July 30, 2023. Date of online publication: September 1, 2023.

This work was jointly supported by the Major Program of National Natural Science Foundation of China (No. U2166601) and the General Program of National Natural Science Foundation of China (No. 52077196).

R. Sadiq, Z. Wang (corresponding author), and D. Gan are with the College of Electrical Engineering, Zhejiang University, Hangzhou 310058, China (e-mail: rehan.sadiq@zju.edu.cn; z.wang@zju.edu.cn; dgan@zju.edu.cn).

C. Y. Chung is with The Hong Kong Polytechnic University, Hong Kong, China (e-mail: c.y.chung@polyu.edu.hk).

C. Tong is with State Grid Zhejiang Electric Power Company, Hangzhou 310007, China (e-mail: tcz88123@163.com)

DOI: 10.35833/MPCE.2023.000347

ing stress in the mechanical structure of the turbine [12], [13]. Alternatively, modifying the reactive power control loop of PMSGs also delivered a similar performance in comparison to active power control [2], [12]. Some studies explored the performance of DC-link voltage modulation for damping purposes [3], [6], [13], [14]. The analysis showed that better control efficiency can be accomplished by adopting this approach without perturbing the PMSG dynamics [3]. Furthermore, the simultaneous regulation of DC-link voltage with the speed and pitch angle control loops also exhibited efficient power modulation capability, justified by achieving significant improvement in the damping of LFOs [15]. Therefore, we also emphasizes modulating the DC-link voltage control loop of the grid-side converter (GSC).

The previously discussed studies [2]-[6], [10], [13], [15] mainly focused on designing a damping controller for a nominal operating point (OP). Meanwhile, it is investigated that the damping contribution from the PMSG is sensitive to varying OPs owing to deviations in wind speed, generation/load variations, and topological changes (i.e., tie-line outages) in the power network [16]. Therefore, the controller designed for a specific OP may not provide optimal damping performance for a wide operating region. A multi-polytope adaptive wide-area damping controller (WADC) based on Kalman filters was proposed to damp LFOs at unknown OPs [1]. Regarding uncertainties in power system operation, time delays, and communication failure of WADC channels, a WADC was designed using a hybrid particle swarm algorithm and the algebraic Riccati equation [17], [18]. Another WADC, based on a machine learning approach, provided enhanced robustness under a wide operating range [19]. Besides, few works illustrated the performance of robust damping controllers for wind farms, designed by solving the linear matrix inequality (LMI) conditions considering power system uncertainties [20]-[22].

Regarding H_∞ static output feedback (SOF) methods, the WADC synthesized by satisfying Lyapunov stability criteria via the LMI framework, provided sufficient damping of oscillation considering time delays and load uncertainties [20], [23]. Compared to state feedback [19], [22] and higher-order dynamic output feedback controllers [21], a robust SOF controller, having a simpler structure based on the static gain with no essential requirement for measuring system states, can be easily implemented in practice with low cost [24], [25]. Furthermore, expressing the H_∞ SOF control problem as a proportional-integral-derivative (PID) based design yields a more practical and widely adopted control structure for power system applications [26], [27]. Also, some LMI-based schemes [1], [22] accomplish the damping objective of the critical modes by satisfying the pole-placement constraint, which may compromise the damping of other modes [17]. Additionally, the LMI techniques described in [20], [27] are based on a common Lyapunov function for the entire uncertain model, which is a conservative approach. Therefore, in view of the above-mentioned studies and assessing their shortcomings, this paper adopts less conservative LMI conditions to design an H_∞ SOF-based PID controller for the PMSG by assuring robust stability via parameter-dependent Lyapunov function [24], [25]. The key contributions of the current research are as follows.

1) A coordinated robust PID-based control approach is presented for the PMSG to damp LFOs, while addressing power system uncertainties due to varying operating conditions.

2) The uncertainties in the power system are expressed via a polytopic model formed by linearizing the system at typical OPs. Consequently, the designed controller ensures robustness across a wide operating range by encompassing uncertainties at the design stage. The coordinated control for multiple wind farms with different sets of polytopes is realized by sequentially designing the damping controllers using the proposed approach.

3) The structure of the robust controller is composed of static PID gains, determined by first formulating the design problem as an SOF control methodology and then solving LMI conditions to simultaneously guarantee robust stability and H_∞ performance level for the whole polytope using the parameter-dependent Lyapunov function. The comparative simulation results corroborate the superior performance of the proposed approach under various uncertainties and disturbances.

The rest of this work is structured as follows. Section II illustrates the modeling and control of the PMSG-interfaced power system. The uncertain model formulation and robust controller design are demonstrated in Section III. The case study, comprising polytopic construction, eigenvalue analysis, and simulation results, is described in Section IV. Finally, concluding remarks are presented in Section V.

II. Modeling and Control of PMSG-interfaced Power Systems

The complete modeling of the power system is implemented by incorporating the differential and algebraic equations, representing the dynamics of SGs, exciter, governor, network, and PMSG. To represent SGs of the system, the sixth-order sub-transient model is adopted together with two exciter models (IEEE ST1A and DC4B) [28]. The detailed dynamics of a PMSG-based wind farm comprises of turbine mechanical and aerodynamic model, blade pitch control, generator, and back-to-back converter with a grid side filter, as shown in Fig. 1. The WT characteristics and aerodynamic model are referred to [29]. The mechanical dynamics of the drive train are represented by the lumped-mass model [30]. The dynamics of the PMSG in the *d-q* reference are expressed as:

$$L_q \frac{\mathrm{d}i_{sq}}{\mathrm{d}t} = -R_s i_{sq} - L_d i_{sd}\omega_r + \phi_m \omega_r - v_{sq} \tag{1}$$

$$L_d \frac{\mathrm{d}i_{sd}}{\mathrm{d}t} = -R_s i_{sd} + L_q i_{sq}\omega_r - v_{sd} \tag{2}$$

$$T_e = -L_d i_{sd} i_{sq} + \phi_m i_{sq} + L_q i_{sq} i_{sd} \tag{3}$$

$$P_s = v_{sq} i_{sq} + v_{sd} i_{sd} \tag{4}$$

$$Q_s = v_{sq} i_{sd} - v_{sd} i_{sq} \tag{5}$$

where R_s is the stator resistance; ω_r is the generator speed; v_{sd}, v_{sq}, i_{sd}, i_{sq}, and L_d, L_q are the *d-q*-axis components of the stator voltage, current, and inductance, respectively; ϕ_m is the rotor flux; and T_e, P_s, and Q_s are the electrical torque,

stator active, and reactive power, respectively. The generator output is connected to the machine-side converter (MSC), which provides active power/torque and reactive power control using q- and d-axis control loops, respectively, as shown in Fig. 1. The DC-link dynamic model is represented as:

$$\dot{v}_{dc}=\frac{1}{C_{dc}v_{dc}}(P_s-P_{gsc}) \tag{6}$$

where $P_{gsc}=v_{gq}i_{gq}+v_{gd}i_{gd}$ is the active power delivered to the grid by the GSC, and v_{gd}, v_{gq} and i_{gd}, i_{gq} are the d-q-axis components of voltage and current of the GSC, respectively; and C_{dc} and v_{dc} are the DC-link capacitance and voltage, respectively. The GSC is coupled with the grid through the RL filter. By adopting a cascaded control structure, the q-axis outer control loop regulates the DC-link voltage, whereas the d-axis outer control loop adjusts the reactive power of the converter Q_g transferring to the grid, as depicted in Fig. 1. where PI stands for proportional-integral.

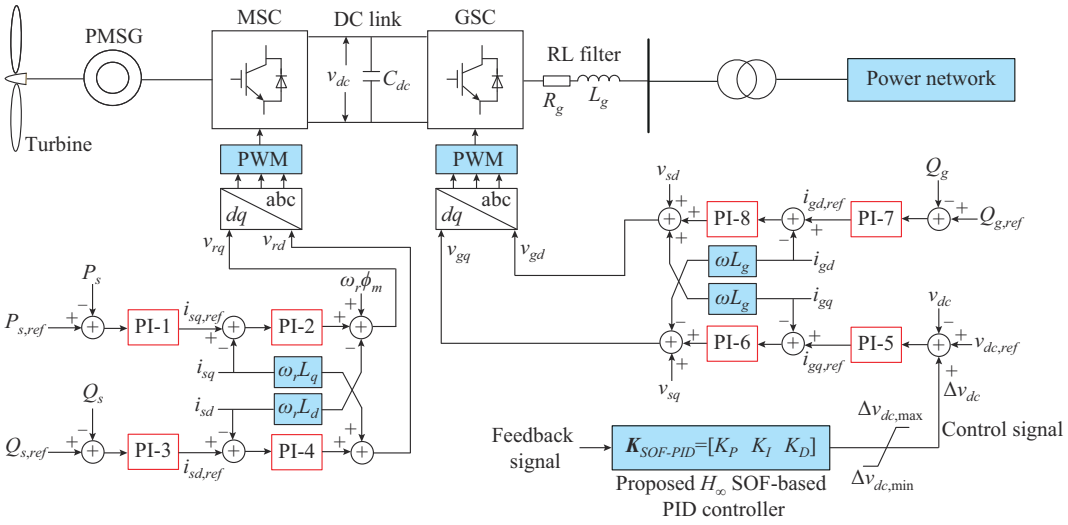

Fig. 1. Configuration and control of PMSG.

The dynamic model of the GSC in the d-q reference frame, by aligning the q axis with the grid voltage, is given as:

$$\frac{L_g}{\omega_{el}}\frac{\mathrm{d}i_{gq}}{\mathrm{d}t}=-R_g i_{gq}+\omega_s L_g i_{gd}+v_{gq}-v_{sq} \tag{7}$$

$$\frac{L_g}{\omega_{el}}\frac{\mathrm{d}i_{gd}}{\mathrm{d}t}=-R_g i_{gd}-\omega_s L_g i_{gq}+v_{gd}-v_{sd} \tag{8}$$

where ω_{el} is the system base speed; ω_s is the synchronous speed; and R_g and L_g are the grid-side filter resistance and inductance, respectively.

As shown in Fig. 1, the injected control signal Δv_{dc} is provided by the proposed H_∞ SOF-based PID controller to modulate the DC-link voltage. This v_{dc} modulation eventually provides the power modulation through the GSC by dynamically altering the electrostatic energy stored in the DC-link capacitance C_{dc}. Because of the large C_{dc} values in modern PMSG-based WTs, a small variation in v_{dc} is enough to provide power modulation, which is injected in the grid via the GSC to support oscillation damping [15]. The parameters of the WTG are provided in Appendix A.

III. Uncertain Model Formulation and Robust Controller Design

A. Uncertainty Modeling and Robust Stability Analysis

The OPs of the power system vary with irregular wind speeds, different generation/load requirements, and topological changes in the network. Subsequently, the damping characteristics of LFOs are also affected. In this respect, the traditional damping controller designed for a particular OP or a single linear time-invariant (LTI) model may not provide adequate performance for diverse OPs. Fortunately, the use of polytopic design can successfully resolve this issue by incorporating multiple LTI models. A polytope can be regarded as a convex combination of its vertices, where each vertex denotes a single LTI model linearized at a certain OP. In this way, the polytopic design ensures that uncertainties are taken into account during the design process. The uncertain augmented LTI system that belongs to a convex polytopic domain can be described by the following state-space model [25]:

$$\dot{\boldsymbol{x}}=\boldsymbol{A}_i\boldsymbol{x}+\boldsymbol{B}_{1i}\boldsymbol{w}+\boldsymbol{B}_{2i}\boldsymbol{u} \tag{9}$$

$$\boldsymbol{z}=\boldsymbol{C}_{1i}\boldsymbol{x}+\boldsymbol{D}_{11i}\boldsymbol{w}+\boldsymbol{D}_{12i}\boldsymbol{u} \tag{10}$$

$$\boldsymbol{y}=\boldsymbol{C}_{2i}\boldsymbol{x}+\boldsymbol{D}_{21i}\boldsymbol{w} \tag{11}$$

$$\boldsymbol{S}_i=[\boldsymbol{A}_i,\boldsymbol{B}_{1i},\boldsymbol{B}_{2i},\boldsymbol{C}_{1i},\boldsymbol{C}_{2i},\boldsymbol{D}_{11i},\boldsymbol{D}_{12i},\boldsymbol{D}_{21i}] \tag{12}$$

where $\boldsymbol{x}\in\mathbf{R}^n$, $\boldsymbol{u}\in\mathbf{R}^p$, $\boldsymbol{w}\in\mathbf{R}^m$, $\boldsymbol{y}\in\mathbf{R}^r$, and $\boldsymbol{z}\in\mathbf{R}^q$ denote the state variables, control input (i.e., Δv_{dc}), external disturbance, measured output, and controlled output, respectively; $\boldsymbol{A}_i$, $\boldsymbol{B}_{1i}$, $\boldsymbol{B}_{2i}$, $\boldsymbol{C}_{1i}$, $\boldsymbol{C}_{2i}$, $\boldsymbol{D}_{11i}$, $\boldsymbol{D}_{12i}$, and $\boldsymbol{D}_{21i}$ are the uncertain augmented LTI system matrices; and $\boldsymbol{S}_i$ denotes the i^{th} vertex ($i=1,2,\ldots,N$) with N being the total number of vertices. The convex combination of these vertices constitutes a polytope $\boldsymbol{\Omega}$ described as:

$$\boldsymbol{\Omega}=\mathbb{C}\{\boldsymbol{S}_1,\boldsymbol{S}_2,\ldots,\boldsymbol{S}_N\}=\left\{\sum_{i=1}^{N}\alpha_i\boldsymbol{S}_i:\sum_{i=1}^{N}\alpha_i=1,\alpha_i\geq 0\right\} \tag{13}$$

where $\mathbb{C}$ and α_i denote the convex hull and polytopic coordi-

nate, respectively. The geometric illustration of polytopic uncertainty for polytope $\boldsymbol{\Omega}$ is depicted in Fig. 2, where blue circles denote vertices, which represent different LTI models with each model corresponding to a different OP, and red circles indicate the convex combinations. Because of polytopic convexity, once the control law is formulated by satisfying LMI constraints for all vertices, the designed controller is capable of assuring robust performance for all the OPs lying within the polytope.

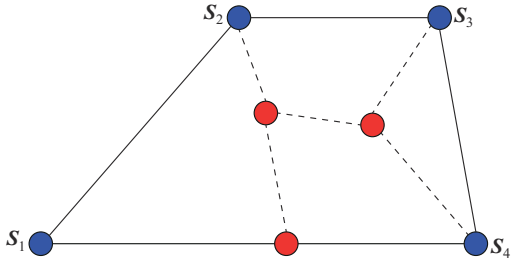

Fig. 2. Geometric illustration of polytopic uncertainty for polytope $\boldsymbol{\Omega}$.

For an uncertain polytopic model (9)-(11), robust stability analysis involves assuring asymptotic (Hurwitz) stability, i.e., the eigenvalues of all matrices $\boldsymbol{A}_i \in \boldsymbol{S}_i$ have negative real part. The Lyapunov stability theorem is a well-known method for assessing this requirement, as it ensures Hurwitz stability of the system by employing a Lyapunov function $\boldsymbol{V}(\boldsymbol{x})=\boldsymbol{x}^{\mathrm{T}}\boldsymbol{Q}\boldsymbol{x}$ with a fixed positive definite matrix $\boldsymbol{Q}=\boldsymbol{Q}^{\mathrm{T}}>\boldsymbol{0}$ [25]. Instead of guaranteeing quadratic stability, where a common Lyapunov function is used for entire polytopic model [1], [17]-[22], [27], less conservative stability can be established by using sufficient LMI conditions based on the parameter-dependent matrix $\boldsymbol{Q}_i=\boldsymbol{Q}_i^{\mathrm{T}}>\boldsymbol{0}$ via Lyapunov function $\boldsymbol{V}(\boldsymbol{x})=\boldsymbol{x}^{\mathrm{T}}\boldsymbol{Q}_i\boldsymbol{x}$ such that $\dot{\boldsymbol{V}}(\boldsymbol{x})<\boldsymbol{0}$ for all $\boldsymbol{x}(t)\neq\boldsymbol{0}$ [24].

B. H_∞ SOF Controller

The formulation of an SOF controller $\boldsymbol{K}$, structured as a static gain matrix, is presented as (14) or (15).

$$\boldsymbol{u}=\boldsymbol{K}\boldsymbol{y} \tag{14}$$

$$\boldsymbol{u}=\boldsymbol{K}(\boldsymbol{C}_{2i}\boldsymbol{x}+\boldsymbol{D}_{21i}\boldsymbol{w}) \tag{15}$$

Using (9)-(11) and (15), the closed-loop system becomes:

$$\dot{\boldsymbol{x}}=\boldsymbol{A}_i\boldsymbol{x}+\boldsymbol{B}_{1i}\boldsymbol{w}+\boldsymbol{B}_{2i}\boldsymbol{K}(\boldsymbol{C}_{2i}\boldsymbol{x}+\boldsymbol{D}_{21i}\boldsymbol{w}) \tag{16}$$

$$\boldsymbol{z}=\boldsymbol{C}_{1i}\boldsymbol{x}+\boldsymbol{D}_{11i}\boldsymbol{w}+\boldsymbol{D}_{12i}\boldsymbol{K}(\boldsymbol{C}_{2i}\boldsymbol{x}+\boldsymbol{D}_{21i}\boldsymbol{w}) \tag{17}$$

$$\begin{bmatrix}\dot{\boldsymbol{x}}_{cl}\\ \boldsymbol{z}\end{bmatrix}=\begin{bmatrix}\boldsymbol{A}_{cl,i} & \boldsymbol{B}_{cl,i}\\ \boldsymbol{C}_{cl,i} & \boldsymbol{D}_{cl,i}\end{bmatrix}\begin{bmatrix}\boldsymbol{x}_{cl}\\ \boldsymbol{w}\end{bmatrix} \tag{18}$$

where $\boldsymbol{x}_{cl}=\boldsymbol{x}$; $\boldsymbol{A}_{cl,i}=\boldsymbol{A}_i+\boldsymbol{B}_{2i}\boldsymbol{K}\boldsymbol{C}_{2i}$; $\boldsymbol{B}_{cl,i}=\boldsymbol{B}_{1i}+\boldsymbol{B}_{2i}\boldsymbol{K}\boldsymbol{D}_{21i}$; $\boldsymbol{C}_{cl,i}=\boldsymbol{C}_{1i}+\boldsymbol{D}_{12i}\boldsymbol{K}\boldsymbol{C}_{2i}$; and $\boldsymbol{D}_{cl,i}=\boldsymbol{D}_{11i}+\boldsymbol{D}_{12i}\boldsymbol{K}\boldsymbol{D}_{21i}$.

The control objective refers to the design of H_∞ SOF-based PID controller of the form (14) for the continuous-time LTI system (9)-(11) such that the closed-loop system (16) and (17) is asymptotically stable when $\boldsymbol{w}=\boldsymbol{0}$ and satisfies the H_∞ performance requirement described as follows:

$$\left\|\boldsymbol{T}_{zw}(s)\right\|_\infty<\gamma \tag{19}$$

$$\left\|\boldsymbol{T}_{zw}(s)\right\|_\infty=\max_{w}\left|\boldsymbol{T}_{zw}(\mathrm{j}\omega)\right| \tag{20}$$

$$\boldsymbol{T}_{zw}(s)=\boldsymbol{C}_{cl,i}(s\boldsymbol{I}-\boldsymbol{A}_{cl,i})^{-1}\boldsymbol{B}_{cl,i}+\boldsymbol{D}_{cl,i} \tag{21}$$

where $\left\|\boldsymbol{T}_{zw}(s)\right\|_\infty$ represent the H_∞ norm of the closed-loop transfer function $\boldsymbol{T}_{zw}(s)$ from $\boldsymbol{w}$ to $\boldsymbol{z}$; and $\boldsymbol{I}$ is the identity matrix. From (19)-(21), it is inferred that, for any $\gamma>0$, H_∞ norm of the system $\boldsymbol{T}_{zw}(s)$ should be minimized to guarantee the robust performance subject to various disturbances. The following lemmas will be used to formulate sufficient conditions for the uncertain model stabilization via SOF controller [25].

Lemma 1 For a scalar β and matrices $\boldsymbol{P}$, $\boldsymbol{V}$, $\boldsymbol{Y}$, and $\boldsymbol{A}$, the below-mentioned expressions, i. e., (22) and (23), are equivalent [25].

$$\begin{bmatrix}\boldsymbol{V} & *\\ \beta\boldsymbol{P}^{\mathrm{T}}+\boldsymbol{Y}\boldsymbol{A} & -\beta\boldsymbol{Y}-\beta\boldsymbol{Y}^{\mathrm{T}}\end{bmatrix} \tag{22}$$

$$\begin{cases}\boldsymbol{V}<\boldsymbol{0}\\ \boldsymbol{V}+\boldsymbol{A}^{\mathrm{T}}\boldsymbol{P}^{\mathrm{T}}+\boldsymbol{P}\boldsymbol{A}<\boldsymbol{0}\end{cases} \tag{23}$$

where * denotes the respective symmetric terms in block matrices.

Lemma 2 For a closed-loop system (16) and (17) with a scalar $\gamma>0$, if the matrix $\boldsymbol{K}$ and the parameter-dependent matrix $\boldsymbol{Q}_i$ satisfies (24), then the asymptotic stability of the system is ensured with minimized H_∞ norm equal to γ.

$$\begin{bmatrix}\boldsymbol{He}((\boldsymbol{A}_i+\boldsymbol{B}_{2i}\boldsymbol{K}\boldsymbol{C}_{2i})\boldsymbol{Q}_i) & * & *\\ (\boldsymbol{B}_{1i}+\boldsymbol{B}_{2i}\boldsymbol{K}\boldsymbol{D}_{21i})^{\mathrm{T}} & -\gamma^2\boldsymbol{I} & *\\ (\boldsymbol{C}_{1i}+\boldsymbol{D}_{12i}\boldsymbol{K}\boldsymbol{C}_{2i})\boldsymbol{Q}_i & \boldsymbol{D}_{11i}+\boldsymbol{D}_{12i}\boldsymbol{K}\boldsymbol{D}_{21i} & -\boldsymbol{I}\end{bmatrix}<\boldsymbol{0} \tag{24}$$

where $\boldsymbol{He}(\boldsymbol{A})=\boldsymbol{A}+\boldsymbol{A}^{\mathrm{T}}$.

Considering Lemmas 1 and 2, the LMI condition for synthesizing SOF controller (14) can be expressed by the following theorem [25].

Theorem 1 For the system (16) and (17), given that $\gamma>0$ with known scalar parameters β and ρ, if there exists a Lyapunov matrix $\boldsymbol{Q}$ and the matrices $\boldsymbol{X}$ and $\boldsymbol{Y}$ with substitution $\boldsymbol{K}\boldsymbol{Y}=\boldsymbol{X}$, then the following LMIs must hold:

$$\boldsymbol{\mathcal{M}}_{ii}<\boldsymbol{0}\quad i=1,2,\ldots,N \tag{25}$$

$$\boldsymbol{\mathcal{M}}_{ij}+\boldsymbol{\mathcal{M}}_{ji}<\boldsymbol{0}\quad i<j,i,j=1,2,\ldots,N \tag{26}$$

$$\boldsymbol{Q}_j>\boldsymbol{0}\quad j=1,2,\ldots,N \tag{27}$$

$$\boldsymbol{\mathcal{M}}_{ii}=\begin{bmatrix}\boldsymbol{He}(\boldsymbol{A}_i\boldsymbol{Q}_i+\boldsymbol{B}_{2i}\boldsymbol{X}\boldsymbol{\mathcal{F}}^i_{p\times n}) & * & * & *\\ \boldsymbol{B}_{1i}^{\mathrm{T}}+\boldsymbol{D}_{21i}^{\mathrm{T}}\boldsymbol{X}^{\mathrm{T}}\boldsymbol{B}_{2i}^{\mathrm{T}} & -\gamma^2\boldsymbol{I} & * & *\\ \boldsymbol{C}_{1i}\boldsymbol{Q}_i+\rho\boldsymbol{\mathcal{F}}^{\mathrm{T}}_{q\times p}\boldsymbol{X}^{\mathrm{T}}\boldsymbol{B}_{2i}^{\mathrm{T}}+\boldsymbol{D}_{12i}\boldsymbol{X}\boldsymbol{\mathcal{F}}^i_{p\times n} & \boldsymbol{D}_{11i}+\boldsymbol{D}_{12i}\boldsymbol{X}\boldsymbol{D}_{21i} & -\boldsymbol{I}+\boldsymbol{He}(\rho\boldsymbol{D}_{12i}\boldsymbol{X}\boldsymbol{\mathcal{F}}_{p\times q}) & *\\ \beta\boldsymbol{X}^{\mathrm{T}}\boldsymbol{B}_{2i}^{\mathrm{T}}+\boldsymbol{C}_{2i}\boldsymbol{Q}_i-\boldsymbol{Y}\boldsymbol{\mathcal{F}}^i_{p\times n} & \boldsymbol{D}_{21i}-\boldsymbol{Y}\boldsymbol{D}_{21i} & \beta\boldsymbol{X}^{\mathrm{T}}\boldsymbol{D}_{12i}^{\mathrm{T}}-\rho\boldsymbol{Y}\boldsymbol{\mathcal{F}}_{p\times q} & -\beta\boldsymbol{Y}-\beta\boldsymbol{Y}^{\mathrm{T}}\end{bmatrix} \tag{28}$$

$$\boldsymbol{\mathcal{M}}_{ij}=\begin{bmatrix} \boldsymbol{He}(\boldsymbol{A}_i\boldsymbol{Q}_j+\boldsymbol{B}_{2i}\boldsymbol{X}\boldsymbol{\mathcal{F}}^j_{p\times n}) & * & * & * \\ \boldsymbol{B}^{\mathrm{T}}_{1i}+\boldsymbol{D}^{\mathrm{T}}_{21j}\boldsymbol{X}^{\mathrm{T}}\boldsymbol{B}^{\mathrm{T}}_{2i} & -\gamma^2\boldsymbol{I} & * & * \\ \boldsymbol{C}_{1i}\boldsymbol{Q}_j+\rho\boldsymbol{\mathcal{F}}^{\mathrm{T}}_{q\times p}\boldsymbol{X}^{\mathrm{T}}\boldsymbol{B}^{\mathrm{T}}_{2i}+\boldsymbol{D}_{12i}\boldsymbol{X}\boldsymbol{\mathcal{F}}^j_{p\times n} & \boldsymbol{D}_{11i}+\boldsymbol{D}_{12i}\boldsymbol{X}\boldsymbol{D}_{21j} & -\boldsymbol{I}+\boldsymbol{He}(\rho\boldsymbol{D}_{12i}\boldsymbol{X}\boldsymbol{\mathcal{F}}_{p\times q}) & * \\ \beta\boldsymbol{X}^{\mathrm{T}}\boldsymbol{B}^{\mathrm{T}}_{2i}+\boldsymbol{C}_{2i}\boldsymbol{Q}_j-\boldsymbol{Y}\boldsymbol{\mathcal{F}}^j_{p\times n} & \boldsymbol{D}_{21i}-\boldsymbol{Y}\boldsymbol{D}_{21j} & \beta\boldsymbol{X}^{\mathrm{T}}\boldsymbol{D}^{\mathrm{T}}_{12i}-\rho\boldsymbol{Y}\boldsymbol{\mathcal{F}}_{p\times q} & -\beta\boldsymbol{Y}-\beta\boldsymbol{Y}^{\mathrm{T}} \end{bmatrix} \tag{29}$$

$$\boldsymbol{\mathcal{F}}_{p\times q}=\begin{cases} \boldsymbol{I} & p=q \\ [\boldsymbol{I}_{p\times p} \quad \boldsymbol{0}_{p\times(q-p)}] & p<q \\ \begin{bmatrix} \boldsymbol{I}_{q\times q} \\ \boldsymbol{0}_{(p-q)\times q} \end{bmatrix} & p>q \end{cases} \tag{30}$$

$$\boldsymbol{\mathcal{F}}^j_{p\times n}=\begin{cases} (\boldsymbol{C}_2\boldsymbol{C}_2^{\mathrm{T}})^{-1}\boldsymbol{C}_2 & \text{fixed } \boldsymbol{C}_2 \text{ and full rank} \\ \boldsymbol{C}_2 & \text{fixed } \boldsymbol{C}_2 \text{ and non - full rank} \\ \boldsymbol{C}_{2j} & \text{non - fixed } \boldsymbol{C}_2 \end{cases} \tag{31}$$

The SOF gain matrix is given as:

$$\boldsymbol{K}_{SOF}=\boldsymbol{X}\boldsymbol{Y}^{-1} \tag{32}$$

The selection of two scalar variables β and ρ provides additional degree of freedom in the solution space to satisfy the LMI conditions [25]. The values can be selected freely in such a way that the resulting PID gains produce adequate damping of dominant modes.

C. Design of Robust PID-based Damping Controller

For design of the robust PID-based damping controller, the structure of the controller (14) is modified as:

$$\boldsymbol{u}=K_P\boldsymbol{y}+K_I\int\boldsymbol{y}\mathrm{d}t+K_D\frac{\mathrm{d}\boldsymbol{y}}{\mathrm{d}t} \tag{33}$$

where K_P, K_I, and K_D are the PID gains to be determined using SOF control law $\boldsymbol{u}=\boldsymbol{K}\boldsymbol{y}$. To accomplish this, we can rewrite (33) as [26]:

$$\boldsymbol{u}=[K_P \quad K_I \quad K_D]\left[\boldsymbol{y} \quad \int\boldsymbol{y}\mathrm{d}t \quad \frac{\mathrm{d}\boldsymbol{y}}{\mathrm{d}t}\right]^{\mathrm{T}} \tag{34}$$

Accordingly, the calculation of the SOF gain matrix in (32) can be expressed as:

$$\boldsymbol{K}_{SOF\text{-}PID}=[K_P \quad K_I \quad K_D]=\boldsymbol{X}\boldsymbol{Y}^{-1} \tag{35}$$

Hence, the SOF control problem is converted into a conventional PID-based control problem by performing integral and derivative actions on the measured output signal, thereby augmenting the $\boldsymbol{C}_{2i}$ matrix of (11) with additional output vectors. In practice, the derivative controller could be affected by sensor noise. To avoid this, the derivative term is combined with a first-order (low-pass) filter to reject the high-frequency noise. Hence, the overall transfer function of the derivative block becomes $K_D\frac{sN_d}{s+N_d}$, where N_d represents the filter coefficient. The cut-off frequency of the filter is determined by the frequency modes of interest [27]. In view of LFO range (0.1-2.0 Hz), the value $N_d=1$ is chosen in the this paper. Finally, the design objective is to find the static gain matrix $\boldsymbol{K}_{SOF\text{-}PID}$ by assuring the asymptotic stability of the uncertain closed-loop system (16) and (17) via the LMIs (25)-(27) with H_∞ norm γ. The overall structure of the proposed robust PID-based damping controller, including a typical high-pass washout filter [21], is shown in Fig. 3.

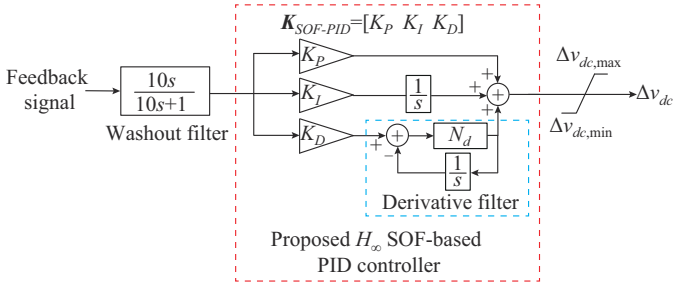

Fig. 3. Overall structure of proposed robust PID-based damping controller.

D. Controller Implementation

The creation of an uncertain polytopic model and the procedure to synthesize the controller can be illustrated via the following steps.

Step 1: establish a set of OPs that describes the wide operating region of a power system.

Step 2: select a suitable feedback signal for the controller.

Step 3: create vertices of a polytope by linearizing the power system at each OP.

Step 4: perform small-signal stability analysis to find the weakly damped modes associated with each vertex.

Step 5: apply the model reduction method to obtain reduced-order system models.

Step 6: develop a polytope by combining reduced order uncertain system matrices (12), attained by means of the augmented state-space realization (9)-(11).

Step 7: construct controller $\boldsymbol{K}_{SOF\text{-}PID}$ (35) by solving the optimization problem to minimize the H_∞ norm γ subject to the inequality constraints (25)-(27). The solution to this optimization problem is obtained by using the built-in MATLAB command "*mincx*" of the LMI control toolbox.

Step 8: after forming a closed-loop system with the first controller, use the model as an open-loop plant for the sequential design of the second controller by repeating *Steps 1* to *7*.

Step 9: validate the effectiveness and robustness of the controller by performing eigenvalue analysis and non-linear simulations for various uncertainties and disturbances.

IV. Case Study

The proposed approach for the coordinated design of wind farm damping controllers is validated using a modified 5-area 68-bus benchmark system, as shown in Fig. 4 [31]. The system contains a total of 16 SGs divided into 5 areas. The generators G1-G12 are provided with power system stabilizers to mitigate local modes. During regular power system operation, Area 2 heavily imports power from adjacent regions. Hence, to satisfy power demand in any dynamic load situations, two wind farms (WF1 and WF2), each having 200 MW of rated power and characterized by an aggregated mod-

el of PMSG, are connected in Areas 4 and 3.

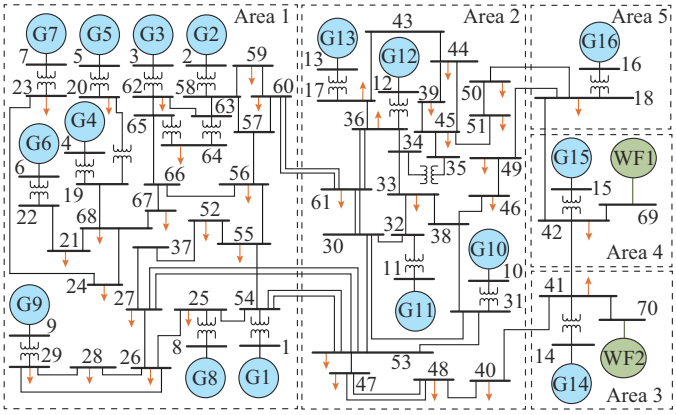

Fig. 4. Modified 5-area 68-bus benchmark system.

A. Polytope Formulation and Eigenvalue Analysis Under Multiple Operating Conditions

To represent uncertainty in power system operation, two different sets of polytopes, each with four vertices (i.e., $i = 1, 2, 3, 4$), stated in Table I and Table II, are considered.

TABLE I
OPs AND DOMINANT MODES FOR POLYTOPE 1

OP	Output power of WF1 (%)	Change in power demand (MW)	Open-loop ζ (%)		Close-loop ζ (%)			
					WF1 control		Coordinated control	
			M_1	M_2	M_1	M_2	M_1	M_2
1	100	No change	3.34	3.69	17.26	5.93	18.99	25.27
2	50	−100 (Area 4)	3.37	3.83	17.04	6.11	18.79	25.14
3	100	+200 (Area 4)	3.29	3.56	17.36	5.80	19.12	25.43
4	75	+400 (Area 4)	3.23	3.46	17.35	5.73	19.18	25.58

TABLE II
OPs AND DOMINANT MODES FOR POLYTOPE 2

OP	Change in power demand (MW)	Topological change (line outage)	Open-loop ζ (%)		Close-loop ζ (%)			
					WF1 control		Coordinated control	
			M_1	M_2	M_1	M_2	M_1	M_2
1	+200 (Area 1)	No change	3.34	3.32	17.27	5.73	19.00	24.99
2	−100 (Area 1)	Line 54-53	3.32	4.26	17.29	8.30	18.98	26.25
3	No change	Line 27-53	3.34	3.76	17.26	6.17	18.99	25.46
4	+400 (Area 1), −400 (Area 5)	No change	3.38	3.42	17.19	5.93	18.86	23.43

These OPs are created by varying the output power of the wind farm and SGs in response to changing load demand in Area 2 followed by topological changes in the 68-bus benchmark system. The choice of these OPs is subject to the convergence of the power flow solution. The topology of the system may change due to contingencies or scheduled maintenance, which could affect the damping properties of LFOs. The impact on inter-area modes will be predominant if the transferring power of the tie-line to remote areas goes out of service. In view of this, two structural changes are incorporated by disconnecting the tie-lines, i.e., Line 54-53 and Line 27-53 between Area 1 and Area 2, as mentioned in Table II for OP2 and OP3. The formation of a single polytope that accommodates a large number of OPs increases complexity and may result in an infeasible solution while solving LMI conditions [22]. Meanwhile, sequentially designed coordinated controllers based on different polytopes, each having distinct OPs, can maintain system stability for a wide range of operating scenarios. The uncertain polytopic model (9)-(11) is then created by linearizing the benchmark system. The small-signal analysis results for the open-loop system, presented in Table I and Table II, show two dominant modes (M_1 and M_2) for each vertex having damping ratios ζ below 5% [31]. From the modal analysis, it is observed that M_1 has the highest participation from G13, G14, and G16; whereas the mode shape of M_2 is related to G15 against G14 and G16. Subsequently, to suppress the critical inter-area modes and improve system damping, this paper focuses on developing a coordinated robust damping control approach for the wind farms at buses 69 and 70.

The input signals for the damping controllers are then selected based on the observability and controllability of the dominant mode to the corresponding feedback signal [32]. By taking the rotor angles of SGs as measured outputs, it is determined that δ_{15} indicates higher residue value for M_1 when the control signal is injected at WF1; whereas the signal δ_{14} is selected for damping of M_2 via WF2. Afterward, the order of the original linearized model associated with each OP is reduced to the 12^{th}-order system. Finally, the sequential coordinated control is accomplished by first designing the PID controller for WF1 considering polytope 1 and then using the closed-loop system with the first controller as an open-loop model to synthesize the second controller for WF2 taking polytope 2 into account [32].

With the closed-loop eigenvalue analysis presented in Table I and Table II, it is demonstrated that WF1 noticeably increases the damping of M_1. On the other hand, M_2 is greatly improved by injecting the controller at WF2, with no adverse effect on other modes. This is also supported by the complex eigenvalue plot depicted in Fig. 5, where M_1 and M_2 are denoted by red and green circles, respectively. Thus, the coordinated control of multiple wind farms provides better damping of inter-area modes for a variety of operating scenarios. The obtained PID gain vectors for WF1 and WF2 are given as (36) and (37), respectively.

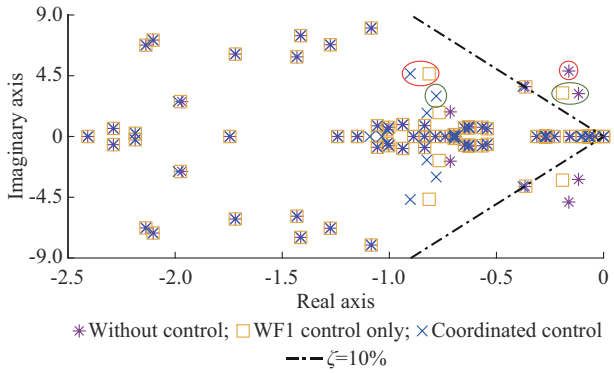

Fig. 5. Complex eigenvalue plot for OP1 of polytope 1.

$$\boldsymbol{K}_{SOF\text{-}PID}=\begin{bmatrix}-1.6848 & -0.0608 & -1.5611\end{bmatrix} \quad (36)$$

$$\boldsymbol{K}_{SOF\text{-}PID}=\begin{bmatrix}-1.3887 & -0.5276 & -0.9938\end{bmatrix} \quad (37)$$

The proposed approach is further tested by conducting time-domain simulations. Besides, a comparative study with an SOF-based PID controller designed via an iterative LMI approach [26] and a mixed H_2/H_∞ WADC [33] is also performed to evaluate the higher robustness of the proposed approach.

B. Time-domain Simulations

1) Case 1: Three-phase Fault Disturbance

This case is tested based on the initial steady-state condition according to OP4 of polytope 1. The wind speed variations for the two wind farms are shown in Fig. 6(a).

The system is simulated by applying a temporary three-phase fault at $t=1$ s at bus 60 for 50 ms duration. The dynamic responses comprising rotor angle difference, rotor speed difference, and line power flow, as shown in Fig. 6(b)-(e), illustrate that large oscillations lasting more than 30 s are observed in the system in the absence of any controller. Nevertheless, oscillations are effectively mitigated within 12 s using the proposed approach. Moreover, from the comparative simulation results, it can be observed that the power system with the proposed approach tends to exhibit fewer dynamic fluctuations and settles oscillations faster compared to other robust damping schemes. The damping contribution from the PMSG is accomplished by dynamically modulating the DC-link voltage, as depicted in Fig. 6(f). The maximum deviation from the steady-state value of v_{dc} is set to be ±0.025 p.u. during transient conditions. Besides, the settling of v_{dc} and other power system variables to a new post-fault steady-state condition is caused by the wind speed changing from its initial value.

2) Case 2: Loss of Generator Disturbance

In view of OP2 and OP3 of polytope 2, two permanent line outages are incorporated in the system during the evaluation of the controller's performance for a contingency condition resulting from the loss of a generator. At $t=1$ s, a dynamic disturbance in Area 1 causes G1 to trip, keeping it out of service for the rest of the simulation interval. The obtained results, demonstrated in Fig. 7, show that the proposed approach delivers robust performance by rapidly mitigating the oscillations under severe disturbance.

3) Case 3: Continuous Load Variation Disturbance

In practice, the power system operates under numerous operating conditions. Therefore, it is not feasible to accommodate all OPs during polytopic model construction at the controller design stage. Meanwhile, the controller must provide acceptable performance for random operating scenarios of the power system. Consequently, the robustness of the controller is tested in this case for any unknown OP that does not belong to polytopes 1 and 2. The new OP is created by assuming 50% and 75% power outputs from WF1 and WF2, respectively, increasing the load of Area 2 at buses 47 and 53 by a total of 600 MW, and disconnecting Line 60-61. The increasing power demand is equally fed by G10, G11, and G14. Later, a dynamic disturbance resulting from the successive tripping of 200 MW load at buses 50 and 51, respectively, occurs at $t=1$ s and $t=15$ s. As a result, the power system oscillations excited by load variation are presented in Fig. 8.

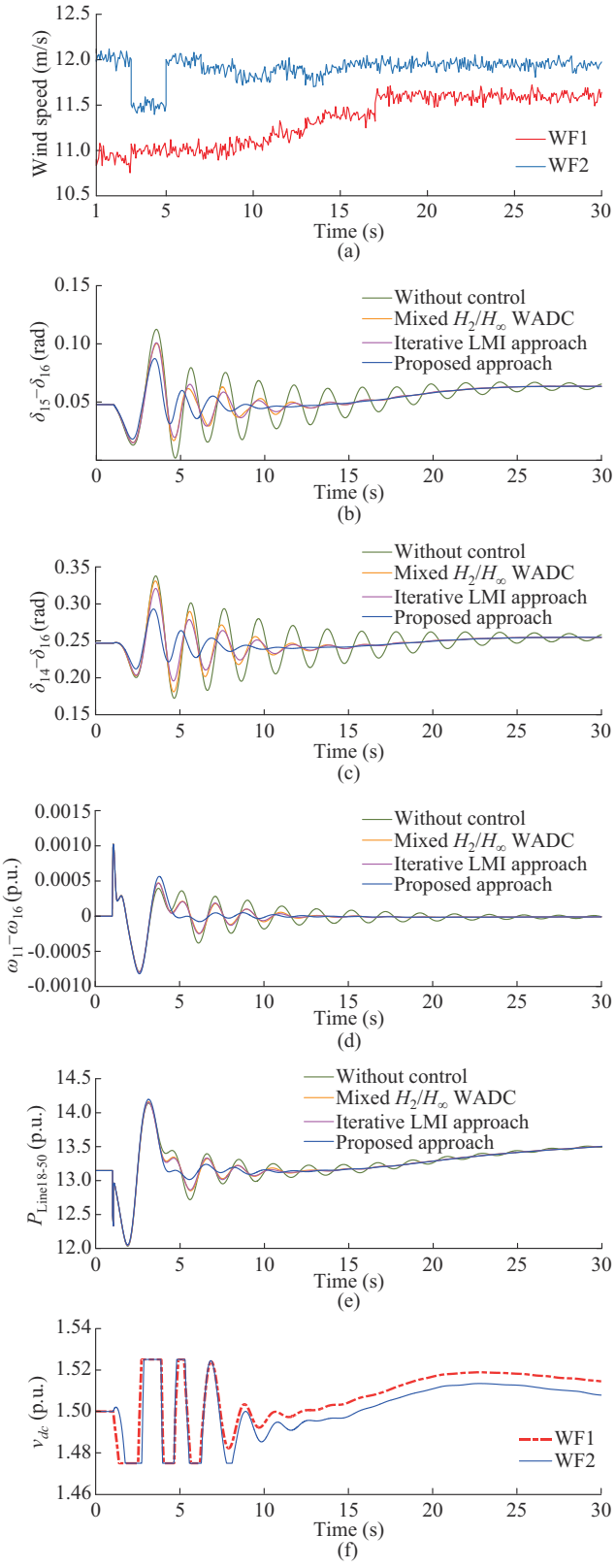

Fig. 6. Simulation results of Case 1. (a) Wind speed variations. (b) Rotor angle difference of G15 and G16. (c) Rotor angle difference of G14 and G16. (d) Rotor speed difference of G11 and G16. (e) Line power flow (Area 5 to Area 2). (f) DC-link voltage modulation of proposed approach.

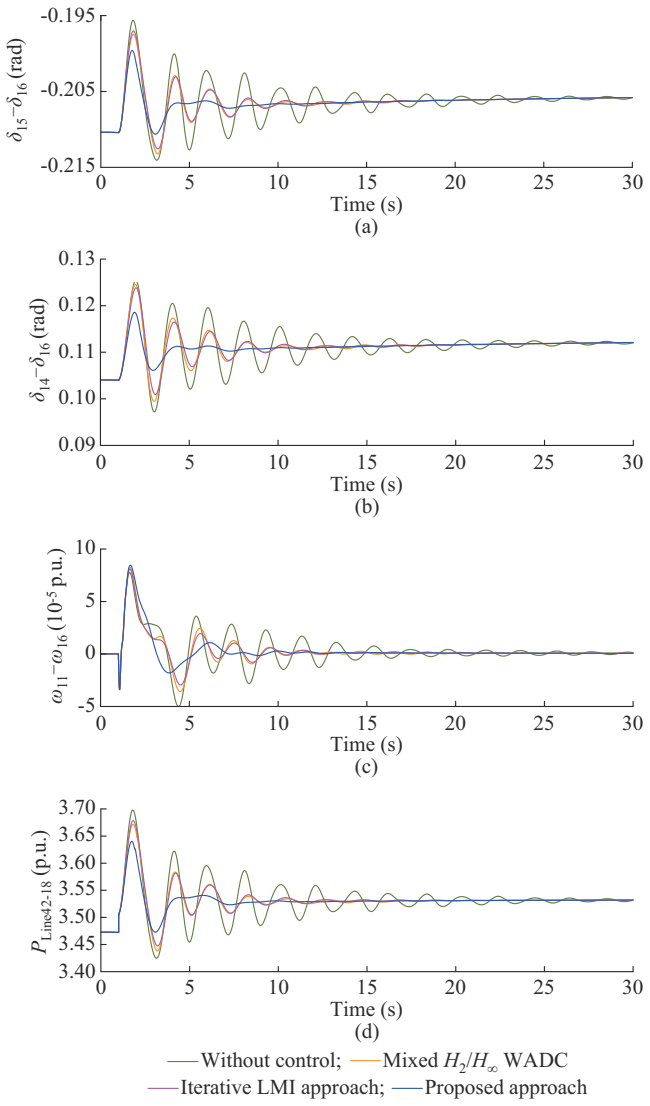

Fig. 7. Simulation results of Case 2. (a) Rotor angle difference of G15 and G16. (b) Rotor angle difference of G14 and G16. (c) Rotor speed difference of G11 and G16. (d) Line power flow (Area 4 to Area 5).

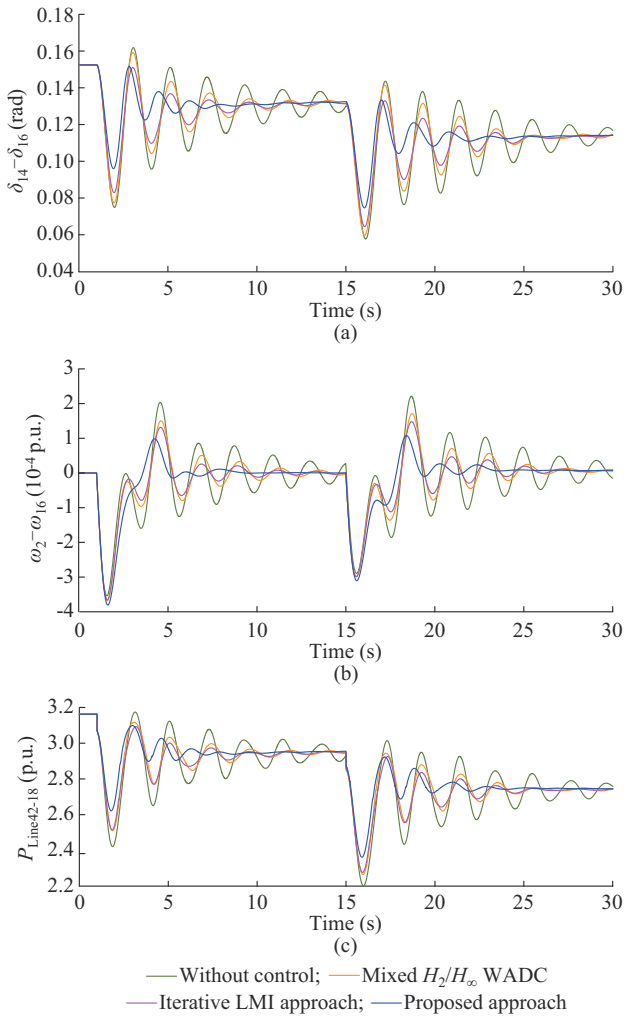

Fig. 8. Simulation results of Case 3. (a) Rotor angle difference of G14 and G16. (b) Rotor speed diference of G2 and G16. (c) Line power flow (Area 4 to Area 5).

The transient responses with the proposed approach evidently show improved damping and settling of the power system at a new OP. Hence, the simulation results validate the higher damping performance and robustness of the controller designed using the proposed approach during continuous load variations and for any random or unknown operating scenario.

C. Performance Evaluation

To quantify the effectiveness of the controller designed using the proposed approach in comparison to using other approaches under various scenarios and disturbances, the performance index J is used [20]:

$$J=\int_0^{T_{sim}}\sum_{i=1}^{N_{gen}}\left|\omega_i-\omega_r\right|t\mathrm{d}t \tag{38}$$

where N_{gen} and T_{sim} denote the total number of generators in the power network and the simulation time, respectively; ω_i is the speed signal of the i^{th} generator; and ω_r is the rotor speed of the generator taken as reference, which in the 68-bus power system is G16.

The lower index value indicates the better performance and robustness of the controller. From Fig. 9, it is observed that J is lowest with the proposed approach for all the test cases conducted in the previous section. This corroborates the superior performance of the proposed approach for different operating scenarios.

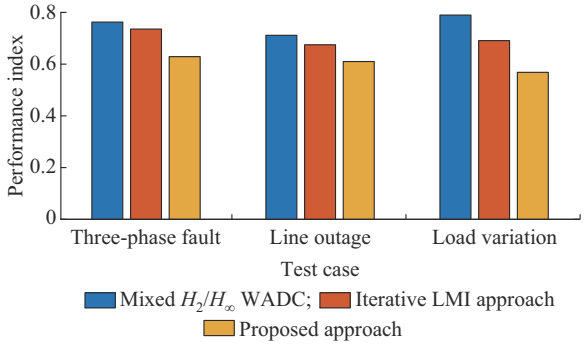

Fig. 9. Performance index value.

V. Conclusion

In this work, we presented a robust damping control ap-

proach for the coordinated control of multiple PMSGs to suppress LFOs considering uncertain polytopic model. The robust PID-based damping controller was designed by minimizing the H_∞ performance objective via satisfying less conservative LMI constraints based on the parameter-dependent Lyapunov function. The conclusions drawn from the current study can be described as follows.

1) The coordinated robust PID-based damping controllers, synthesized using proposed approach, ensured robust stability and successfully mitigated low-frequency inter-area modes by simultaneously guaranteeing robustness under multiple OPs.

2) The static controller gains, for providing the damping function via multiple wind farms in a coordinated manner, are calculated offline by establishing the polytopic models based on diverse operating scenarios, including intermittent wind speed, different generation and load requirements, followed by uncertainty in the topological changes of the power system. Therefore, the controller's parameters remain effective over a wide operating region, even providing satisfactory performance in unknown/random operating conditions.

3) From the time-domain simulation results and quantitative evaluation of the controller's robustness via a performance index, it is concluded that the controller using the proposed approach outperforms the existing SOF-based PID controller and a robust WADC.

4) Unlike other higher-order controllers with several control parameters, the synthesized controller can be preferred for its simple and practically realizable structure.

The application of the proposed approach is not limited to the damping of LFOs only; instead, it has the potential to mitigate other types of oscillations, such as sub-/super-synchronous oscillations, which have also been a critical issue in recent years, particularly with the PMSG-integrated wind power systems. In this respect, the focus of our future research will be on mitigating these oscillations.

APPENDIX A

The parameters of the wind farm are listed below.

1) Turbine and PMSG: the rated wind speed is 12 m/s, the inertia constant H_t is 2 s, the maximum power coefficient $C_{p\max}$ is 0.48, the tip speed ratio λ_{opt} is 8.1, $R_s = 0.0025$ p.u., $L_d = L_q = 0.7$ p.u., and $\phi_m = 1.2$ p.u..

2) DC link and filter: $C_{dc} = 0.3$ p. u., $V_{dc} = 1.5$ p. u., $L_g = 0.0033$ p.u., and $R_g = 0$.

3) PI controllers at MSC side: ① PI-1: $K_P = 0.0001$, $K_I = 0.1$; ② PI-3: $K_P = -100$, $K_I = -1000$; ③ PI-2 and PI-4: $K_P = -90$, $K_I = -1000$.

4) PI controllers at GSC side: ① PI-5: $K_P = -22$, $K_I = -870$; ② PI-7: $K_P = -2$, $K_I = -100$; ③ PI-6 and PI-8: $K_P = 0.3$, $K_I = 200$.

REFERENCES

[1] T. Wang, A. Pal, J. S. Thorp *et al.*, "Use of polytopic convexity in developing an adaptive interarea oscillation damping scheme," *IEEE Transactions on Power Systems*, vol. 32, no. 4, pp. 2509-2520, Jul. 2017.

[2] A. Prakash, P. Singh, K. Kumar *et al.*, "Design of a reduced-order WADC for wind turbine system-integrated power system," *IEEE Transactions on Industry Applications*, vol. 58, no. 3, pp. 3250-3260, May 2022.

[3] E. M. Elhaji and C. J. Hatziadoniu, "Damping tie-line power oscillations by modulation feedback of wind generators," *Electric Power Systems Research*, vol. 143, pp. 739-747, Feb. 2017.

[4] L. Wang and D. N. Truong, "Dynamic stability improvement of four parallel-operated PMSG-based offshore wind turbine generators fed to a power system using a STATCOM," *IEEE Transactions on Power Delivery*, vol. 28, no. 1, pp. 111-119, Jan. 2013.

[5] L. Wang and D. N. Truong, "Stability enhancement of a power system with a PMSG-based and a DFIG-based offshore wind farm using a SVC with an adaptive-network-based fuzzy inference system," *IEEE Transactions on Industrial Electronics*, vol. 60, no. 7, pp. 2799-2807, Jul. 2013.

[6] Z. Zhang, X. Zhao, L. Fu *et al.*, "Stability and dynamic analysis of the PMSG-based WECS with torsional oscillation and power oscillation damping capabilities," *IEEE Transactions on Sustainable Energy*, vol. 13, no. 4, pp. 2196-2210, Oct. 2022.

[7] H. Liu, X. Xie, J. He *et al.*, "Subsynchronous interaction between direct-drive PMSG based wind farms and weak AC networks," *IEEE Transactions on Power Systems*, vol. 32, no. 6, pp. 4708-4720, May 2017.

[8] K. A. Singh, A. Chaudhary, and K. Chaudhary, "Three-phase AC-DC converter for direct-drive PMSG-based wind energy conversion system," *Journal of Modern Power Systems and Clean Energy*, vol. 11, no. 2, pp. 589-598, Mar. 2023.

[9] G. Revel, A. E. Leon, D. M. Alonso *et al.*, "Dynamics and stability analysis of a power system with a PMSG-based wind farm performing ancillary services," *IEEE Transactions on Circuits and Systems I: Regular Papers*, vol. 61, no. 7, pp. 2182-2193, Jul. 2014.

[10] Y. Wang, J. Meng, X. Zhang *et al.*, "Control of PMSG-based wind turbines for system inertial response and power oscillation damping," *IEEE Transactions on Sustainable Energy*, vol. 6, no. 2, pp. 565-574, Apr. 2015.

[11] M. Edrah, X. Zhao, W. Hung *et al.*, "Electromechanical interactions of full scale converter wind turbine with power oscillation damping and inertia control," *International Journal of Electrical Power and Energy Systems*, vol. 135, p. 107522, Aug. 2022.

[12] T. Knüppel, J. N. Nielsen, K. H. Jensen *et al.*, "Power oscillation damping capabilities of wind power plant with full converter wind turbines considering its distributed and modular characteristics," *IET Renewable Power Generation*, vol. 7, no. 5, pp. 431-442, Sept. 2013.

[13] E. M. Elhaji and C. J. Hatziadoniu, "Damping tie line oscillation using permanent magnet wind generators in the Libyan power system," in *Proceedings of 2014 North American Power Symposium (NAPS)*, Pullman, USA, Nov. 2014, pp. 1-6.

[14] H. Geng, D. Xu, B. Wu *et al.*, "Comparison of oscillation damping capability in three power control strategies for PMSG - based WECS," *Wind Energy*, vol. 14, pp. 389-406, Oct. 2010.

[15] E. M. Elhaji and C. J. Hatziadoniu, "Interarea oscillation damping using *H*-infinity control for the permanent magnet wind generator," *Electric Power Systems Research*, vol. 151, pp. 319-328, Oct. 2017.

[16] J. Morato, T. Knuppel, and J. Ostergaard, "Residue-based evaluation of the use of wind power plants with full converter wind turbines for power oscillation damping control," *IEEE Transactions on Sustainable Energy*, vol. 5, no. 1, pp. 82-89, Jan. 2014.

[17] M. E. C. Bento, "A hybrid particle swarm optimization algorithm for the wide-area damping control design," *IEEE Transactions on Industrial Informatics*, vol. 18, no. 1, pp. 592-599, Jan. 2022.

[18] M. E. C. Bento, "Fixed low-order wide-area damping controller considering time delays and power system operation uncertainties," *IEEE Transactions on Power Systems*, vol. 35, no. 5, pp. 3918-3926, Sept. 2020.

[19] P. Gupta, A. Pal, and V. Vittal, "Coordinated wide-area damping control using deep neural networks and reinforcement learning," *IEEE Transactions on Power Systems*, vol. 37, no. 1, pp. 365-376, Jan. 2022.

[20] V. V. G. Krishnan, S. C. Srivastava, and S. Chakrabarti, "A robust decentralized wide area damping controller for wind generators and FACTS controllers considering load model uncertainties," *IEEE Transactions on Smart Grid*, vol. 9, no. 1, pp. 360-372, Jan. 2018.

[21] Y. Pipelzadeh, N. R. Chaudhuri, B. Chaudhuri *et al.*, "Coordinated control of offshore wind farm and onshore HVDC converter for effective power oscillation damping," *IEEE Transactions on Power Systems*, vol. 32, no. 3, pp. 1860-1872, May 2017.

[22] P. Gupta, A. Pal, and V. Vittal, "Coordinated wide-area control of multiple controllers in a power system embedded with HVDC lines," *IEEE Transactions on Power Systems*, vol. 36, no. 1, pp. 648-658,

Jan. 2021.
[23] S. Alghamdi, U. Markovic, O. Stanojev *et al.*, "Wide-area oscillation damping in low-inertia grids under time-varying communication delays," *Electric Power Systems Research*, vol. 189, p. 106629, Dec. 2020.
[24] J. Dong and G. Yang, "Robust static output feedback control synthesis for linear continuous systems with polytopic uncertainties," *Automatica*, vol. 49, no. 6, pp. 1821-1829, Jun. 2013.
[25] X. H. Chang, J. H. Park, and J. Zhou, "Robust static output feedback H_∞ control design for linear systems with polytopic uncertainties," *Systems and Control Letters*, vol. 85, pp. 23-32, Nov. 2015.
[26] H. Bevrani, T. Hiyama, and H. Bevrani, "Robust PID based power system stabiliser: design and real-time implementation," *International Journal of Electrical Power and Energy Systems*, vol. 33, no. 2, pp. 179-188, Feb. 2011.
[27] M. Soliman, A. L. Elshafei, F. Bendary *et al.*, "Robust decentralized PID-based power system stabilizer design using an ILMI approach," *Electric Power Systems Research*, vol. 80, no. 12, pp. 1488-1497, Dec. 2010.
[28] B. C. Pal and C. Balarko, *Robust Control in Power Systems*. New York: Springer, 2005.
[29] M. Rosyadi, S. M. Muyeen, R. Takahashi *et al.*, "New controller design for PMSG based wind generator with LCL-filter considered," in *Proceedings of 20th International Conference on Electrical Machines (ICEM)*, Marseille, France, Nov. 2012, pp. 2112-2118.
[30] F. Wu, X. Zhang, and P. Ju, "Small signal stability analysis and control of the wind turbine with the direct-drive permanent magnet generator integrated to the grid," *Electric Power Systems Research*, vol. 79, pp. 1661-1667, Dec. 2009.
[31] A. K. Singh and B. C. Pal. (2013, Dec.). IEEE PES Task Force on Benchmark Systems for Stability Controls: report on the 68-bus, 16-machine, 5-area system. [Online]. Available: https://www.researchgate.net/publication/311680574
[32] C. Li, J. Deng, and X. Zhang, "Coordinated design and application of robust damping controllers for shunt FACTS devices to enhance small-signal stability of large-scale power systems," *CSEE Journal of Power and Energy Systems*, vol. 3, no. 4, pp. 399-407, Dec. 2017.
[33] Y. J. Isbeih, M. Shawky, E. Moursi *et al.*, "H_∞ mixed-sensitivity robust control design for damping low-frequency oscillations with DFIG wind power generation," *IET Generation, Transmission & Distribution*, vol. 13, no. 19, pp. 4274-4286, Sept. 2019.

Rehan Sadiq received the B.Eng. and M.Eng. degrees from University of Engineering and Technology, Taxila, Pakistan, in 2012 and 2015, respectively. Currently, he is pursuing the Ph.D. degree from College of Electrical Engineering, Zhejiang University, Hangzhou, China. His research interests include power system stability and control with renewable energy penetration and flexible AC transmission system (FACTS).

Zhen Wang received the B.Eng., M.Eng., and Ph.D. degrees from Xi'an Jiaotong University, Xi'an, China, Zhejiang University, Hangzhou, China, and The Hong Kong Polytechnic University, Hong Kong, China, in 1998, 2001, and 2009, respectively. He is currently a Full-time Professor and the Director of Institute of Power and Energy Integration & Intelligence, Zhejiang University. He was the recipient of 2014 Endeavour Research Fellowship sponsored by Australia Government and Visiting Scholar of The University of Western Australia, Perth, Australia. He is an expert member of IEC TC8/SC8B/JWG1 Working Group on Microgrid Operation and Control. He also serves as the Editor of the journal Electronics, and the member of some topical advisory panel. His research interests include power system stability and control, renewable energy integration, and voltage source converter based high-voltage direct current (VSC-HVDC) transmission.

Chi Yung Chung received the B.Eng. (Hons.) and Ph.D. degrees in electrical engineering from The Hong Kong Polytechnic University, Hong Kong, China, in 1995 and 1999, respectively. He is currently the Head of the Department and a Chair Professor in power systems engineering with the Department of Electrical Engineering, The Hong Kong Polytechnic University. He is an IEEE PES Distinguished Lecturer. He was a recipient of the 2021 IEEE Canada P. Ziogas Electric Power Award. He is a Senior Editor of IEEE Transactions on Power Systems, a Consulting Editor of IEEE Transactions on Sustainable Energy, and the Vice Editor-in-Chief of Journal of Modern Power Systems and Clean Energy. His research interests include smart grid technologies, renewable energy, power system stability/control, planning and operation computational intelligence applications, power markets, and electric vehicle charging.

Deqiang Gan received the Ph. D. degree in electrical engineering from Xi'an Jiaotong University, Xi'an, China, in 1994. He has been with the faculty of Zhejiang University, Hangzhou, China, since 2002. He visited the University of Hong Kong, Hong Kong, China, in 2004, 2005 and 2006. He worked for ISO New England, Inc., Holyoke, USA, from 1998 to 2002. He held research positions in Ibaraki University, Ibaraki Prefecture, Japan, University of Central Florida, Orlando, USA, and Cornell University, Ithaca, USA, from 1994 to 1998. He served as an Editor for European Transactions on Electric Power from 2007 to 2014. His research interests include power system stability and control.

Cunzhi Tong received the B.Eng. and M.Eng. degrees from Hefei University of Technology, Hefei, China, and Zhejiang University, Hangzhou, China, in 2011 and 2014, respectively. Currently he is a Senior Engineering in State Grid Zhejiang Electric Power Co., Ltd., Hangzhou, China. His research interests include power system dispatch and operation and project management.